Electronic Supplementary Material (ESI) for Physical Chemistry Chemical Physics.

Supplementary Information for "Elucidating the Interplay of Local and Mesoscale Ion Dynamics and Transport Properties in Aprotic Ionic Liquids"

Tyler Cosby,*,† Christopher D. Stachurski,‡ Robert A. Mantz,¶ Paul C. Trulove,‡ and David P. Durkin*,‡

†*Division of Mathematics and Sciences, University of Tennessee Southern, Pulaski, TN, USA.*

‡*Department of Chemistry, US Naval Academy, Annapolis, MD, USA.*

¶*Army Research Office, Durham, NC, USA.*

E-mail: jcosby3@utsouthern.edu; durkin@usna.edu

Purity of Starting Materials

The purity of the synthesized 1-methyl-3-octylimidazolium chloride was ascertained by proton and carbon NMR measured on a Jeol ECX 400 MHz NMR spectrometer. The purity was estimated at $\geq 99.9\%$. The NMR spectra are provided in Figures 1 and 2. The C_8MIm Cl was further used in the preparation of the C_8MIm $AlCl_4$ and Al_2Cl_7 ILs. On the basis of the purity of the C_8MIm Cl their purities were estimated at $\geq 99\%$. The other ionic liquids were purchased from Iolitec and used as received without further verification of purity. Pu-

rities given in Experimental Methods are reproduced from the product information sheets provided by Iolitec.

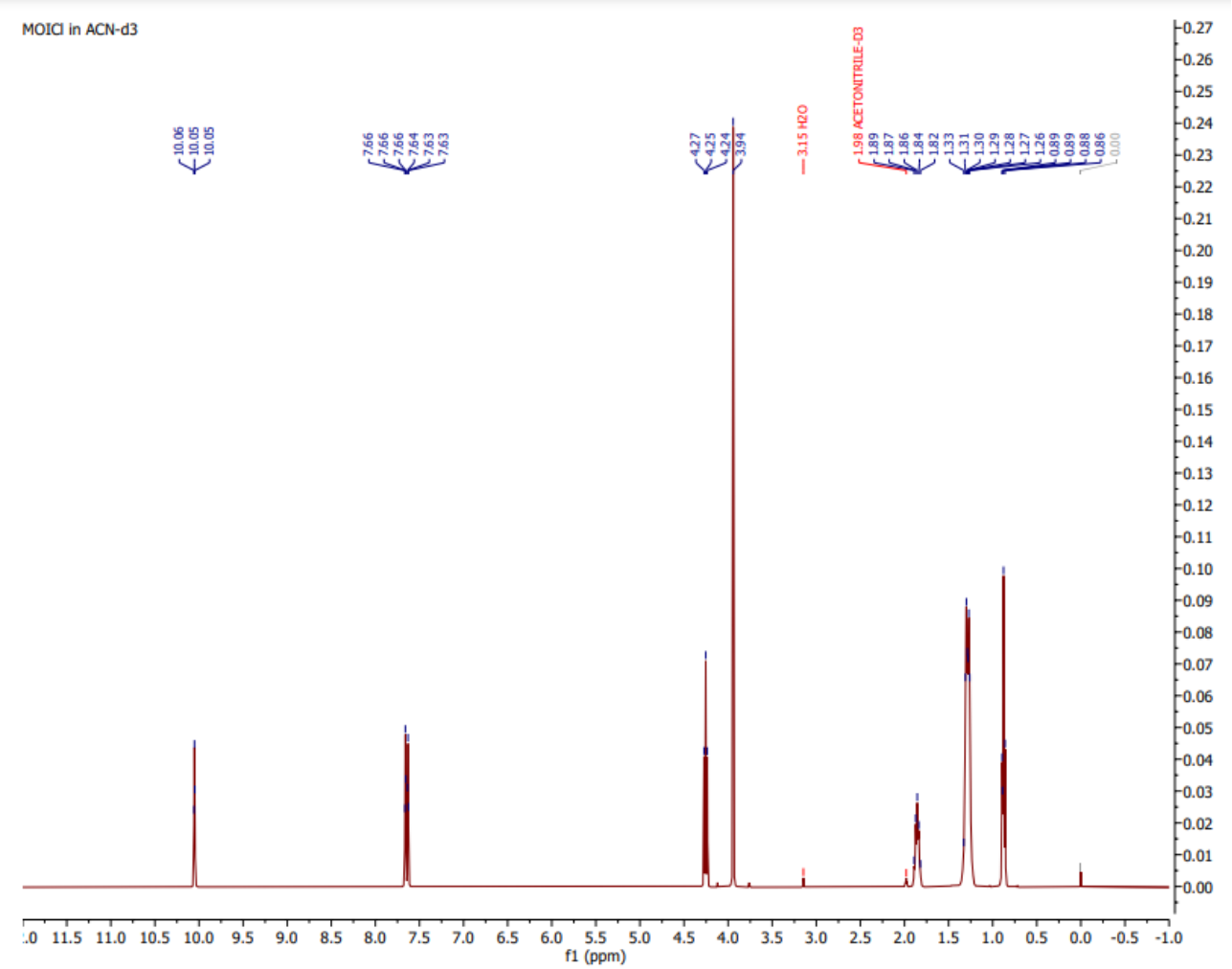

Figure 1: ^{1}H NMR spectrum of C_8MIm Cl in deuterated acetonitrile.

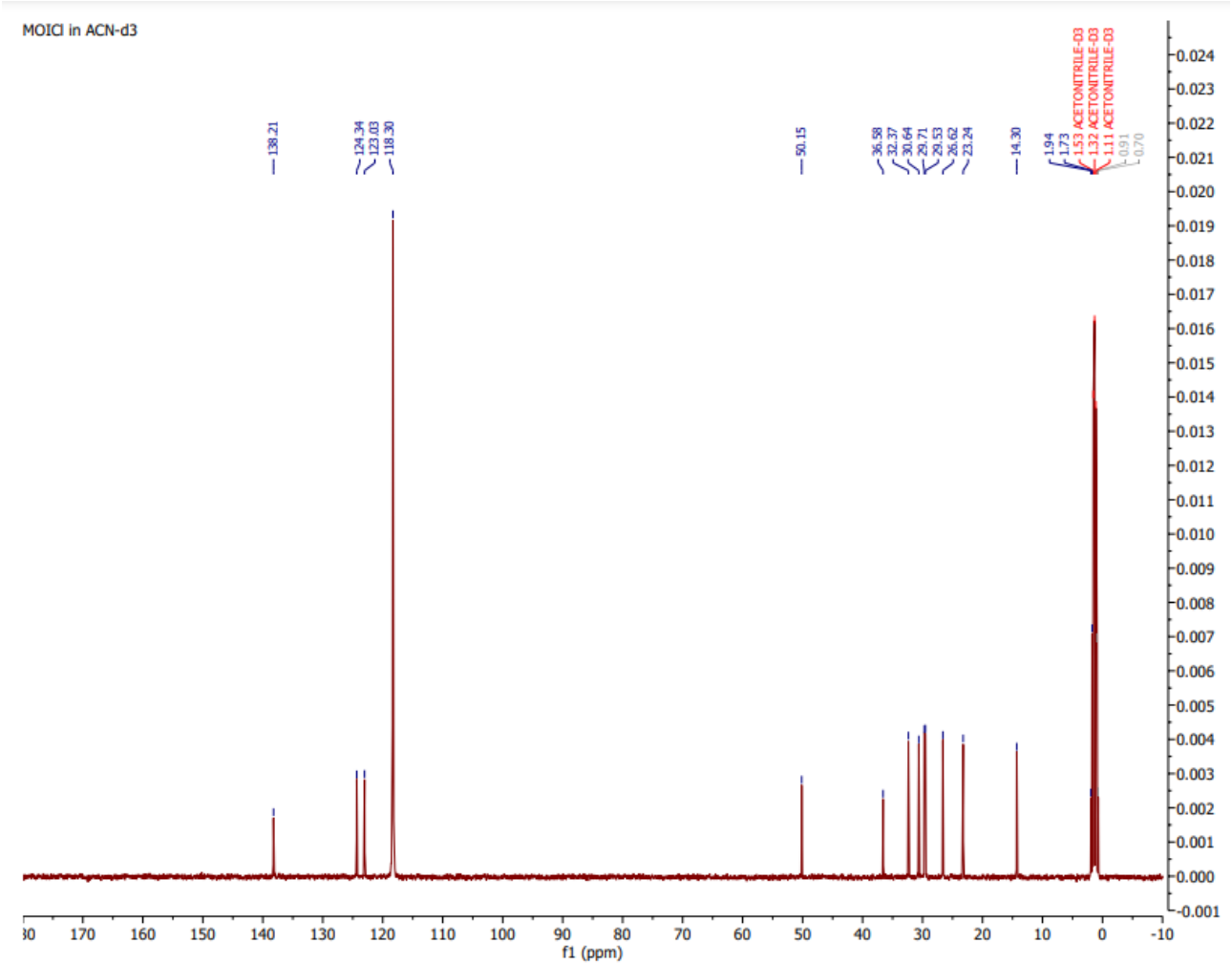

Figure 2: ^{13}C NMR spectrum of C_8MIm Cl in deuterated acetonitrile.

Broadband Dielectric Spectroscopy

The three formalisms in which the dielectric data are presented, $\sigma^*(\omega)$, $M^*(\omega)$, and $\varepsilon^*(\omega)$, are each interrelated.[1] The complex electric modulus is defined as the inverse of complex dielectric permittivity, $M^*(\omega) = \frac{1}{\varepsilon^*(\omega)}$. The imaginary part of complex electric modulus is then given as $M''(\omega) = \frac{\varepsilon''(\omega)}{(\varepsilon'(\omega))^2+(\varepsilon''(\omega))^2}$. The complex conductivity is related to complex dielectric permittivity as $\sigma^*(\omega) = i\omega\varepsilon_0\varepsilon^*(\omega)$, where ε_0 is the permittivity of free space. The real part of complex conductivity is then directly related to the imaginary part of complex dielectric permittivity as $\sigma'(\omega) = \omega\varepsilon_0\varepsilon''(\omega)$.

The broadband dielectric spectra of the 1-methyl-3-octylimidazolium ionic liquids are presented in Supplementary Figures 6, 7, 8, 9, 10, 11, 12, 13, 14.

Relaxation Rates

The temperature dependent relaxation rates were fit using the Vogel-Fulcher-Tammann equation, $\omega_i = \omega_\infty e^{\frac{-DT_0}{T-T_0}}$. The fit parameters are given in Tables 3, 4, 5, 6.

Density

The mass densities measured using an Anton-Paar SVM-3000 Stabinger viscometer, are presented in Supplementary Figure 3.

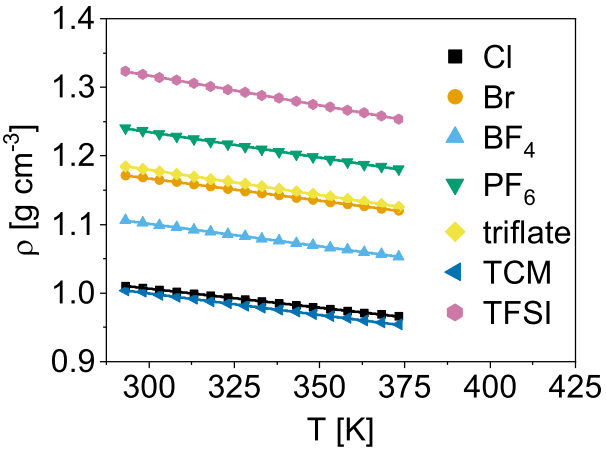

Figure 3: Temperature dependent mass densities of 1-methyl-3-octylimidazolium ionic liquids with the indicated anions. Lines correspond to linear fits, $\rho = mT + b$. Fit parameters are provided in Table 1.

Table 1: Linear fit parameters of temperature dependent mass density.

IL	m	b
C_8MIm Cl	-5.555×10^{-4}	1.1732
C_4MIm Br	-6.439×10^{-4}	1.3601
C_6MIm BF_4	-6.567×10^{-4}	1.2980
C_8MIm PF_6	-7.434×10^{-4}	1.4577
C_6MIm TCM	-6.259×10^{-4}	1.1872
C_8MIm triflate	-7.342×10^{-4}	1.3999
C_8MIm $AlCl_4$	-	-
C_8MIm TFSI	-8.650×10^{-4}	1.5765
C_8MIm Al_2Cl_7	-	-

Differential Scanning Calorimetry

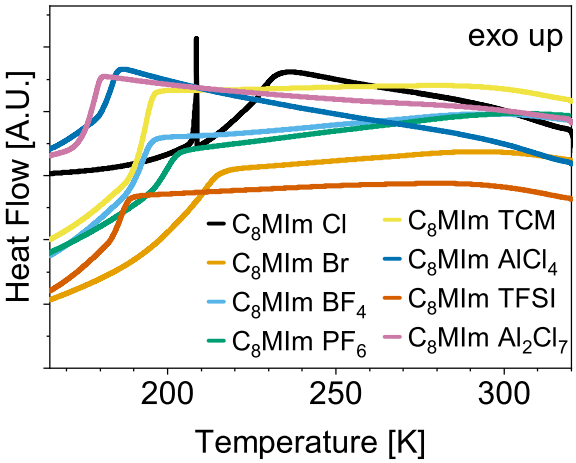

Figure 4: Measured heat flow on cooling of the indicated ILs. Each IL has a glass transition temperature (evidenced by the step decrease in heat flow) and no evidence of crystallization. Cooling rate = 10 °C min^{-1}. The sharp peak below the T_g in the C_8MIm Cl curve is an experimental artifact.

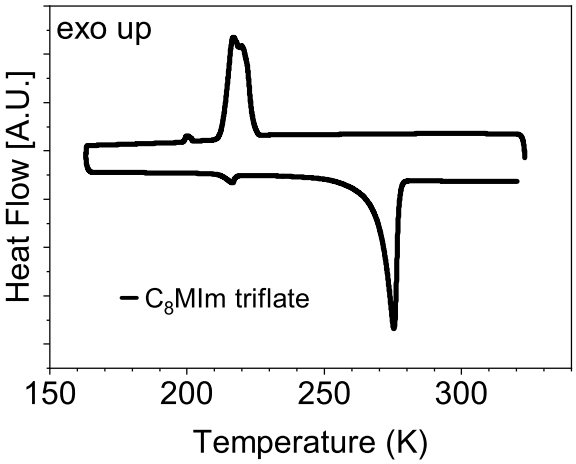

Figure 5: Measured heat flow on cooling of C_8MIm PF_6. This IL undergoes crystallization at 223 K. Cooling/heating rate = 10 °C min^{-1}

High-Frequency Shear Modulus

The values of high-frequency limiting, glassy shear modulus, G_∞, used in Maxwell's relation to calculate the structural relaxation rate, $\omega_\eta = G_\infty/\eta_0$, are presented in Table 2.

Table 2: High-frequency limiting, glassy shear moduli, G_∞, of the investigated ILs.

IL	G_∞ [GPa]
C_8MIm Cl	0.4
C_4MIm Br	0.6
C_6MIm BF_4	0.7
C_8MIm PF_6	0.6
C_6MIm TCM	0.6
C_8MIm triflate	0.4
C_8MIm $AlCl_4$	0.6
C_8MIm TFSI	0.5
C_8MIm Al_2Cl_7	0.5

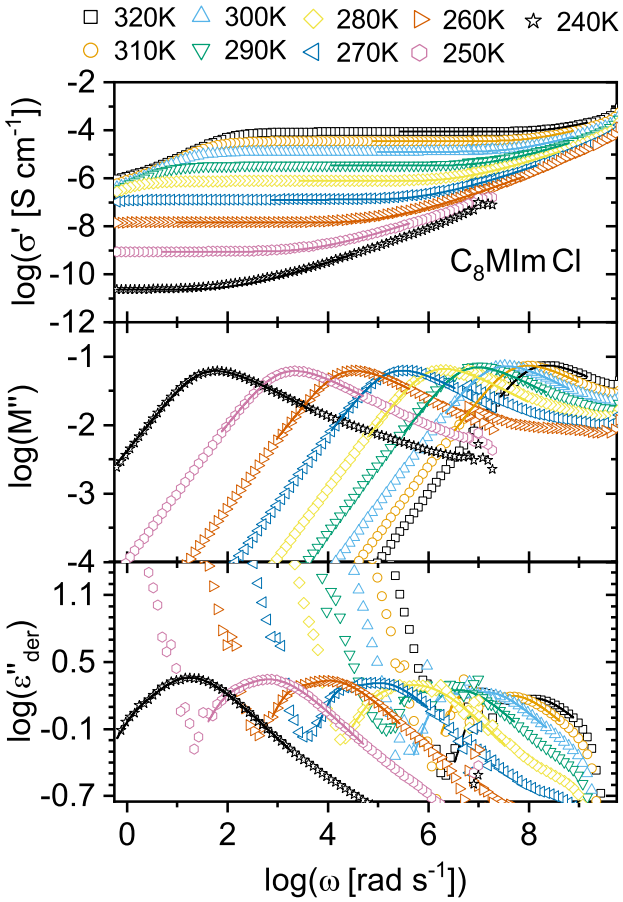

Figure 6: Frequency, ω, and temperature-dependent dielectric spectra of 1-octyl-3-methylimidazolium chloride (C_8MIm Cl). (Top) Real part of complex conductivity, $\sigma'(\omega)$. Lines represent fits by the RBM. Arrows correspond to the ion-hopping rates, ω_{RBM}. (Middle) Imaginary part of complex electric modulus, $M''(\omega)$. Lines represent fits by a single Havriliak-Negami (HN) function. The arrows correspond to the peak maximum, $\omega_{M''}$. (Bottom) Derivative representation of the real part of complex dielectric permittivity, $\varepsilon''_{\mathrm{der}}$. Solid lines represent the total fit obtained by a combination of up to two HN functions. The separate component fit functions are presented as dashed and dotted lines. The shaded areas depict the contribution of the primary, α dielectric relaxation. The arrows correspond to the α-relaxation rate, ω_α.

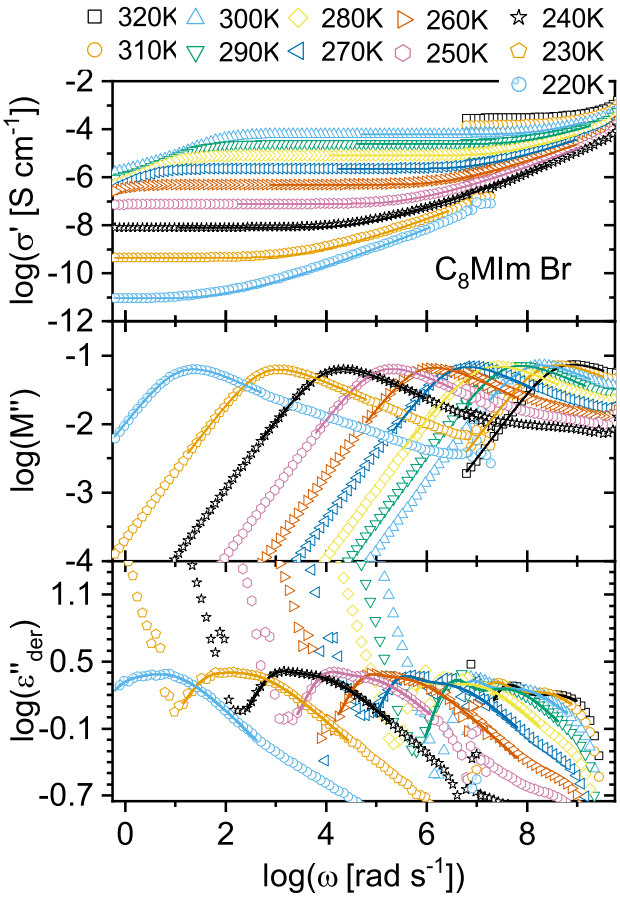

Figure 7: Dielectric spectra of 1-octyl-3-methylimidazolium bromide (C_8MIm Br). (Top) Real part of complex conductivity, $\sigma'(\omega)$. (Middle) Imaginary part of complex electric modulus, $M''(\omega)$. (Bottom) Derivative representation of the real part of complex dielectric permittivity, $\varepsilon''_{\mathrm{der}}$. Lines have the same meaning as in Figure 6.

Table 3: Vogel-Fulcher-Tammann fit parameters obtained from the temperature-dependent Random Barrier Model ion-hopping rates, ω_{RBM}.

IL	ω_∞ [rad s^{-1}]	D	T_0 [K]
C_8MIm Cl	8.94×10^{12}	9.2	177.9
C_8MIm Br	1.11×10^{13}	11.3	155
C_8MIm BF_4	1.41×10^{12}	8.1	150.7
C_8MIm PF_6	2.04×10^{12}	8.8	154.2
C_8MIm TCM	1.11×10^{12}	5.5	161.7
C_8MIm triflate	-	-	-
C_8MIm $AlCl_4$	4.08×10^{11}	5.8	151.6
C_8MIm TFSI	5.59×10^{11}	6.6	151.6
C_8MIm Al_2Cl_7	1.73×10^{11}	4.9	150.1

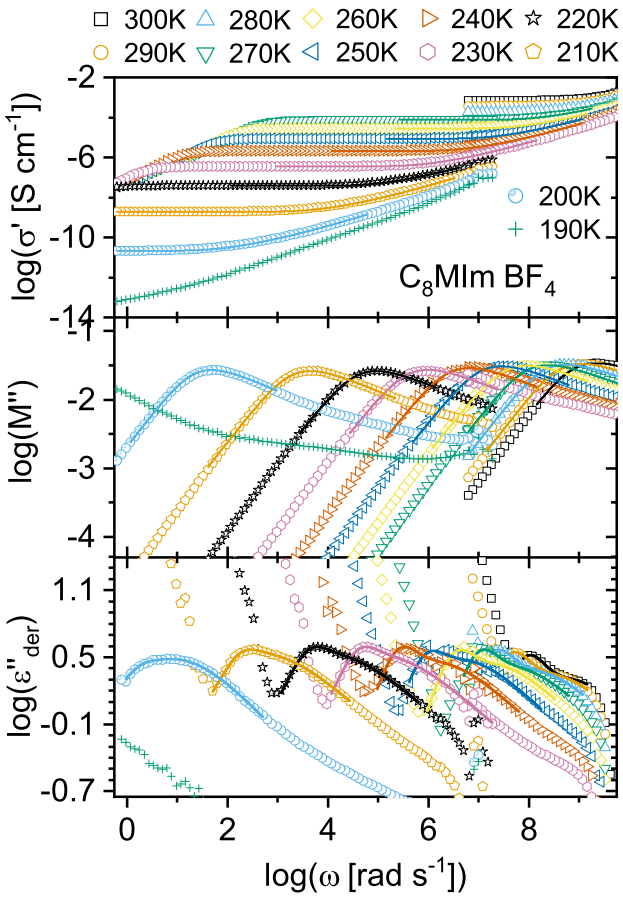

Figure 8: Dielectric spectra of 1-octyl-3-methylimidazolium tetrafluoroborate (C_8MIm BF_4). (Top) Real part of complex conductivity, $\sigma'(\omega)$. (Middle) Imaginary part of complex electric modulus, $M''(\omega)$. (Bottom) Derivative representation of the real part of complex dielectric permittivity, $\varepsilon''_{\mathrm{der}}$. Lines have the same meaning as in Figure 6.

Table 4: Vogel-Fulcher-Tammann fit parameters obtained from the temperature-dependent peak-frequency of M″, $\omega_{\mathrm{M}''}$.

IL	ω_∞ [rad s^{-1}]	D	T_0 [K]
C_8MIm Cl	7.82×10^{13}	10.7	173.4
C_8MIm Br	5.60×10^{12}	11.5	156.8
C_8MIm BF_4	1.27×10^{13}	8.6	150.7
C_8MIm PF_6	2.73×10^{13}	9.0	155.4
C_8MIm TCM	3.26×10^{13}	6.6	159.8
C_8MIm triflate	-	-	-
C_8MIm $AlCl_4$	2.58×10^{12}	5.2	155.8
C_8MIm TFSI	7.01×10^{12}	6.8	152.6
C_8MIm Al_2Cl_7	3.36×10^{12}	4.9	153.1

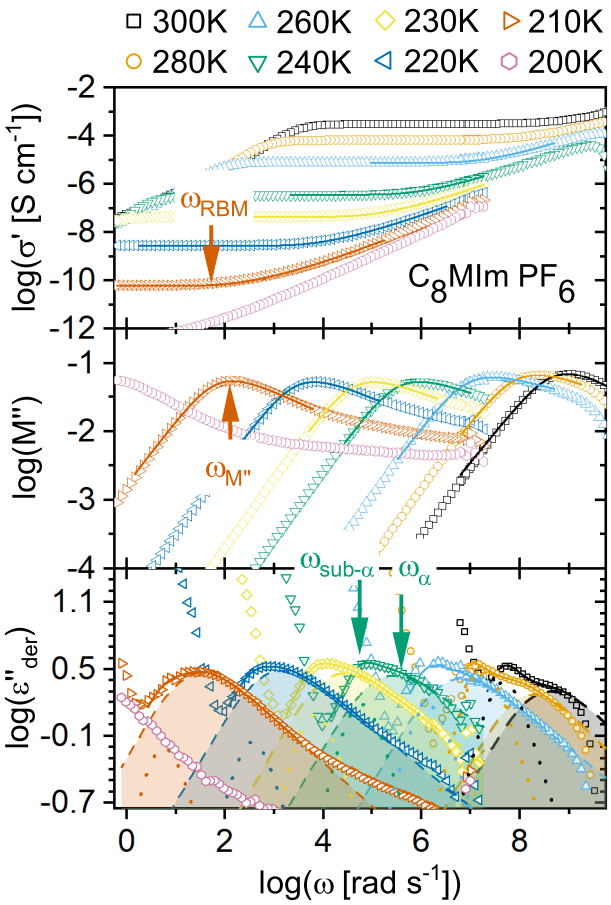

Figure 9: Dielectric spectra of 1-octyl-3-methylimidazolium hexafluorophosphate (C_8MIm PF_6). (Top) Real part of complex conductivity, $\sigma'(\omega)$. (Middle) Imaginary part of complex electric modulus, $M''(\omega)$. (Bottom) Derivative representation of the real part of complex dielectric permittivity, $\varepsilon''_{\mathrm{der}}$. Lines have the same meaning as in Figure 6.

Table 5: Vogel-Fulcher-Tammann fit parameters obtained from the temperature-dependent relaxation rate of the primary, α dielectric relaxation, ω_α.

IL	ω_∞ [rad s^{-1}]	D	T_0 [K]
C_8MIm Cl	1.65×10^{12}	9.2	179.7
C_8MIm Br	2.81×10^{14}	15.2	148.4
C_8MIm BF_4	1.42×10^{13}	9.9	147.9
C_8MIm PF_6	5.25×10^{13}	12.0	147.0
C_8MIm TCM	2.67×10^{13}	7.4	158.0
C_8MIm triflate	-	-	-
C_8MIm $AlCl_4$	2.66×10^{12}	5.6	156.5
C_8MIm TFSI	5.36×10^{12}	7.4	151.3
C_8MIm Al_2Cl_7	2.80×10^{12}	5.5	152.1

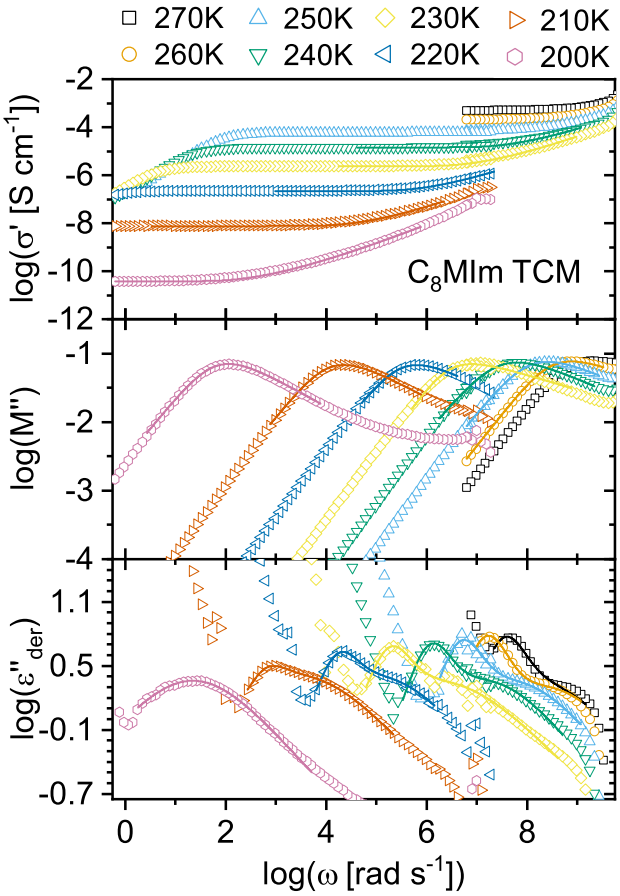

Figure 10: Dielectric spectra of 1-octyl-3-methylimidazolium tricyanomethanide (C_8MIm TCM). (Top) Real part of complex conductivity, $\sigma'(\omega)$. (Middle) Imaginary part of complex electric modulus, $M''(\omega)$. (Bottom) Derivative representation of the real part of complex dielectric permittivity, $\varepsilon''_{\text{der}}$. Lines have the same meaning as in Figure 6.

Table 6: Vogel-Fulcher-Tammann fit parameters obtained from the temperature-dependent rate of the slower, sub-α dielectric relaxation, $\omega_{\text{sub-}\alpha}$.

IL	ω_∞ [rad s^{-1}]	D	T_0 [K]
C_8MIm Cl	1.57×10^{14}	12.0	171.1
C_8MIm Br	2.09×10^{12}	11.2	158.0
C_8MIm BF_4	3.26×10^{11}	7.9	153.0
C_8MIm PF_6	3.70×10^{11}	7.9	159.3
C_8MIm TCM	4.81×10^{11}	6.6	158.8
C_8MIm triflate	-	-	-
C_8MIm $AlCl_4$	1.93×10^{11}	6.2	151.0
C_8MIm TFSI	1.91×10^{11}	6.8	152.2
C_8MIm Al_2Cl_7	2.65×10^{11}	6.3	145.9

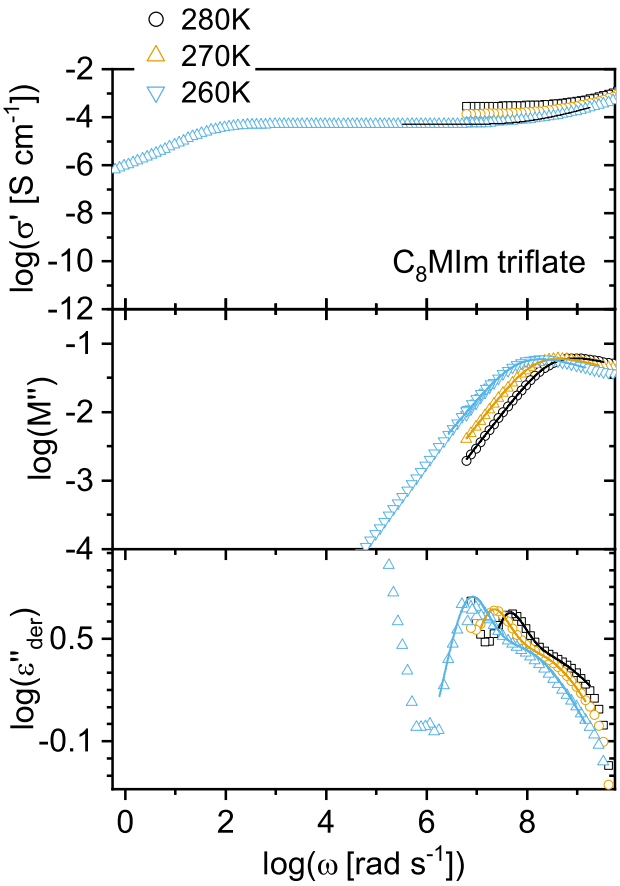

Figure 11: Dielectric spectra of 1-octyl-3-methylimidazolium triflate (C_8MIm triflate). (Top) Real part of complex conductivity, $\sigma'(\omega)$. (Middle) Imaginary part of complex electric modulus, $M''(\omega)$. (Bottom) Derivative representation of the real part of complex dielectric permittivity, $\varepsilon''_{\mathrm{der}}$. Lines have the same meaning as in Figure 6.

Table 7: Vogel-Fulcher-Tammann fit parameters obtained from the temperature-dependent dc ionic conductivities, σ_0 [S cm^{-1}].

IL	σ_∞ [S cm^{-1}]	D	T_0 [K]
C_8MIm Cl	19.2	10.3	174.7
C_8MIm Br	10.5	10.7	158.7
C_8MIm BF_4	3.1	8.4	150.6
C_8MIm PF_6	3.6	8.8	155.0
C_8MIm TCM	2.1	5.5	163.9
C_8MIm triflate	-	-	-
C_8MIm $AlCl_4$	1.2	5.9	152.5
C_8MIm TFSI	1.8	7.1	150.3
C_8MIm Al_2Cl_7	0.67	5.1	151.0

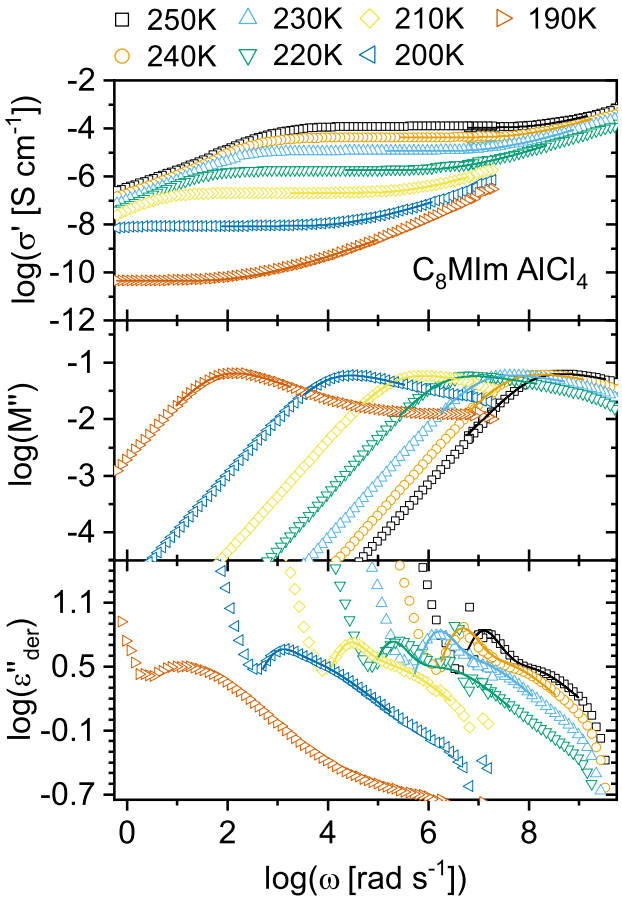

Figure 12: Dielectric spectra of 1-octyl-3-methylimidazolium tetrachlorodialuminate (C_8MIm $AlCl_4$). (Top) Real part of complex conductivity, $\sigma'(\omega)$. (Middle) Imaginary part of complex electric modulus, $M''(\omega)$. (Bottom) Derivative representation of the real part of complex dielectric permittivity, $\varepsilon''_{\mathrm{der}}$. Lines have the same meaning as in Figure 6.

Table 8: Vogel-Fulcher-Tammann fit parameters obtained from the temperature-dependent fluidities, η_0^{-1} [$\mathrm{Pa^{-1}\ s^{-1}}$].

IL	η_∞^{-1} [$\mathrm{Pa^{-1}\ s^{-1}}$]	D	T_0 [K]
C_8MIm Cl	1.1×10^5	10.6	173.5
C_8MIm Br	1.02×10^5	11.2	160.2
C_8MIm BF_4	2.83×10^4	9.3	147.4
C_8MIm PF_6	3.24×10^4	9.5	152.6
C_8MIm TCM	1.43×10^4	5.6	163.3
C_8MIm triflate	-	-	-
C_8MIm $AlCl_4$	1.39×10^4	6.4	149.8
C_8MIm TFSI	2.16×10^4	7.4	149.0
C_8MIm Al_2Cl_7	4.79×10^3	4.6	155.1

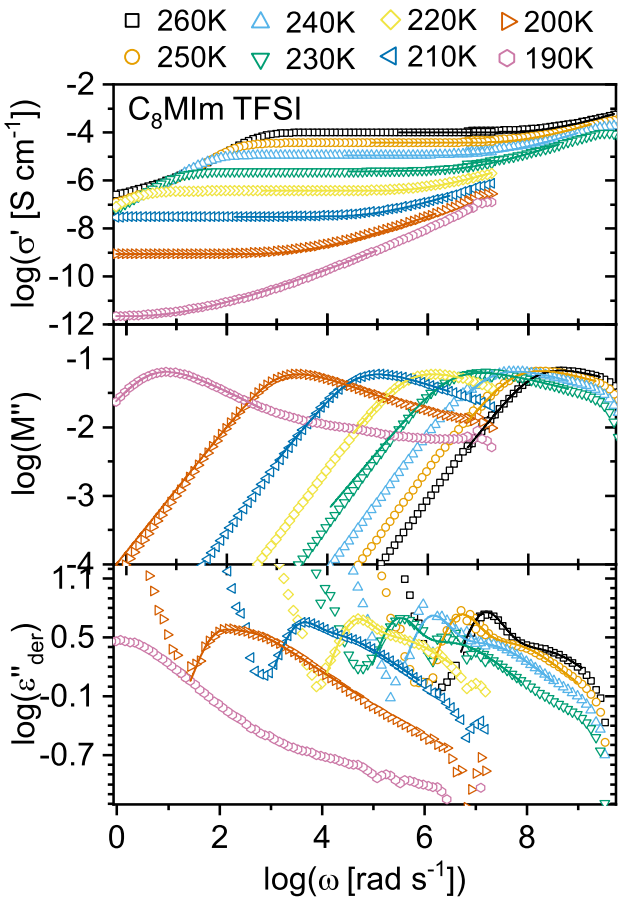

Figure 13: Dielectric spectra of 1-octyl-3-methylimidazolium bis(trifluoromethylsulfonyl)imide (C_8MIm TFSI). (Top) Real part of complex conductivity, $\sigma'(\omega)$. (Middle) Imaginary part of complex electric modulus, $M''(\omega)$. (Bottom) Derivative representation of the real part of complex dielectric permittivity, $\varepsilon''_{\mathrm{der}}$. Lines have the same meaning as in Figure 6.

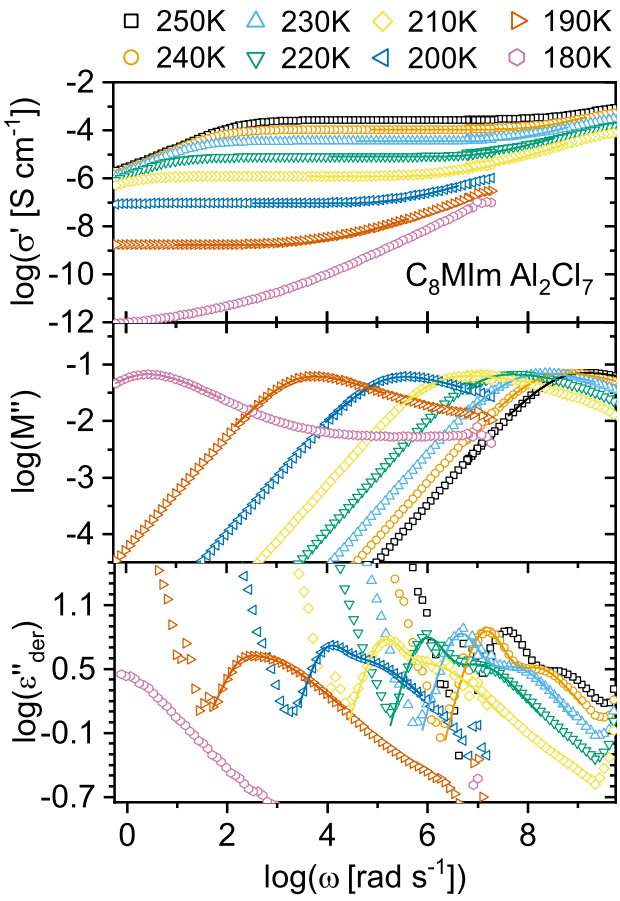

Figure 14: Dielectric spectra of 1-octyl-3-methylimidazolium heptachlorodialuminate (C_8MIm Al_2Cl_7). (Top) Real part of complex conductivity, $\sigma'(\omega)$. (Middle) Imaginary part of complex electric modulus, $M''(\omega)$. (Bottom) Derivative representation of the real part of complex dielectric permittivity, $\varepsilon''_{\rm der}$. Lines have the same meaning as in Figure 6.

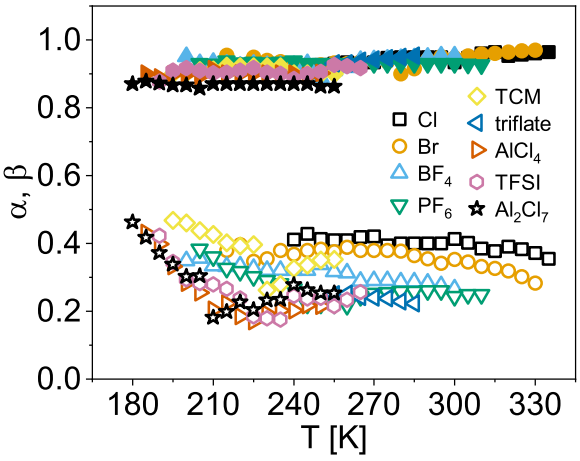

Figure 15: Shape parameters, α (closed symbols) and β (open symbols), of Havriliak-Negami fits applied to the imaginary part of the complex electric modulus.

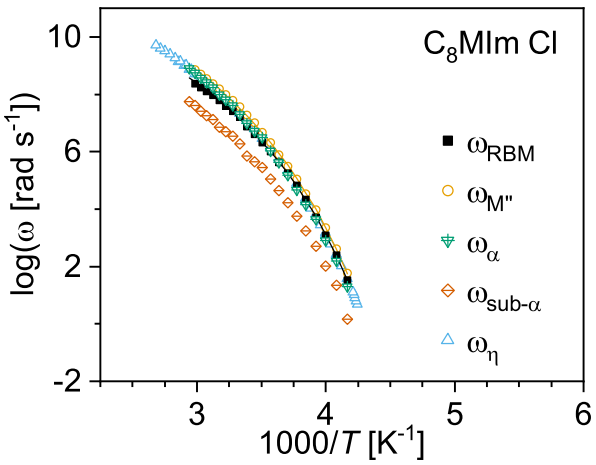

Figure 16: Temperature-dependent relaxation rates of the 1-octyl-3-methylimidazolium chloride (C_8MIm Cl). Rates are obtained by analysis of the dielectric spectra (ω_{RBM}, $\omega_{\mathrm{M''}}$, ω_{α}, $\omega_{\text{sub-}\alpha}$) and rheology ($\omega_{\eta}$). Lines correspond to fits by the VFT equation.

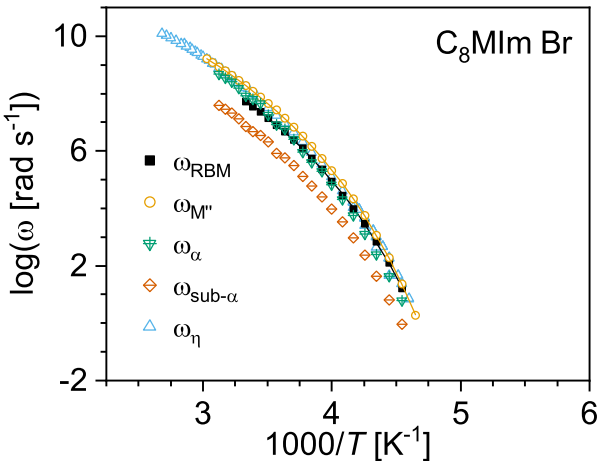

Figure 17: Temperature-dependent relaxation rates of the 1-octyl-3-methylimidazolium bromide (C_8MIm Br). Rates are obtained by analysis of the dielectric spectra (ω_{RBM}, $\omega_{\mathrm{M''}}$, ω_{α}, $\omega_{\text{sub-}\alpha}$) and rheology ($\omega_{\eta}$). Lines correspond to fits by the VFT equation.

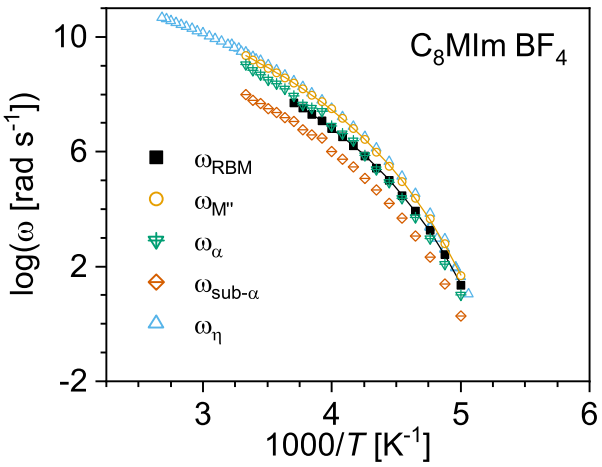

Figure 18: Temperature-dependent relaxation rates of the 1-octyl-3-methylimidazolium tetrafluoroborate (C_8MIm BF_4). Rates are obtained by analysis of the dielectric spectra (ω_{RBM}, $\omega_{\mathrm{M''}}$, ω_α, $\omega_{\text{sub-}\alpha}$) and rheology ($\omega_\eta$). Lines correspond to fits by the VFT equation.

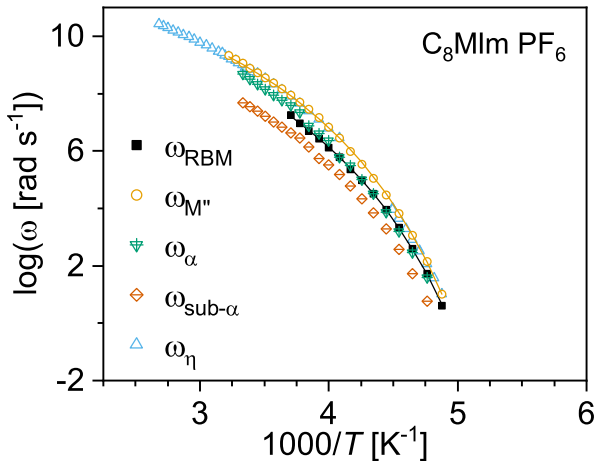

Figure 19: Temperature-dependent relaxation rates of the 1-octyl-3-methylimidazolium hexafluorophosphate (C_8MIm PF_6). Rates are obtained by analysis of the dielectric spectra (ω_{RBM}, $\omega_{\mathrm{M''}}$, ω_α, $\omega_{\text{sub-}\alpha}$) and rheology ($\omega_\eta$). Lines correspond to fits by the VFT equation.

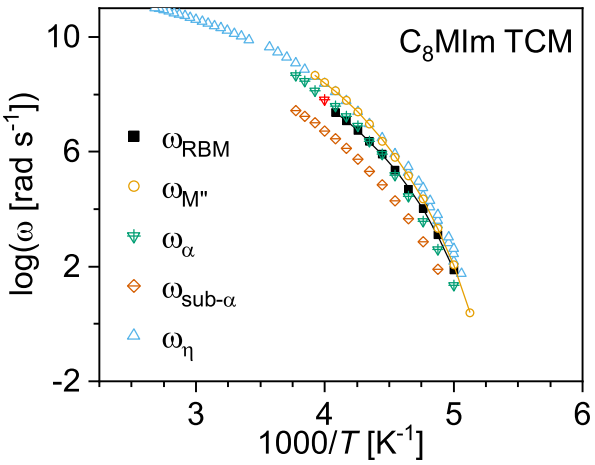

Figure 20: Temperature-dependent relaxation rates of the 1-octyl-3-methylimidazolium tricyanomethanide (C_8MIm TCM). Rates are obtained by analysis of the dielectric spectra (ω_{RBM}, $\omega_{\mathrm{M''}}$, ω_{α}, $\omega_{\text{sub-}\alpha}$) and rheology ($\omega_{\eta}$). Lines correspond to fits by the VFT equation.

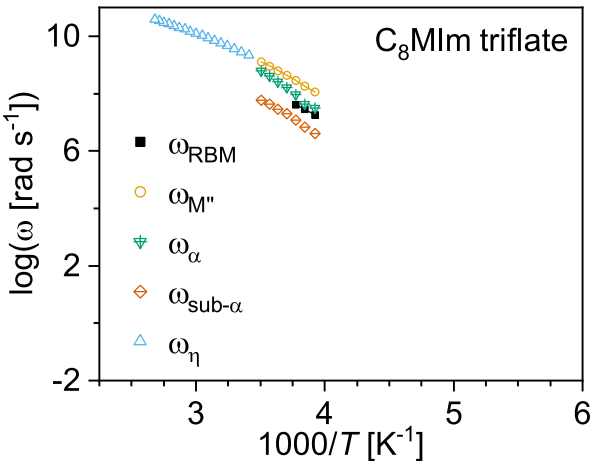

Figure 21: Temperature-dependent relaxation rates of the 1-octyl-3-methylimidazolium triflate (C_8MIm triflate). Rates are obtained by analysis of the dielectric spectra (ω_{RBM}, $\omega_{\mathrm{M''}}$, ω_{α}, $\omega_{\text{sub-}\alpha}$) and rheology ($\omega_{\eta}$). Lines correspond to fits by the VFT equation.

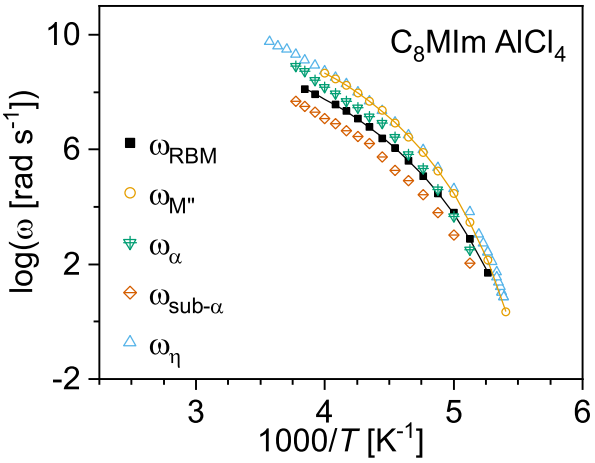

Figure 22: Temperature-dependent relaxation rates of the 1-octyl-3-methylimidazolium tetrachlorodialuminate (C_8MIm $AlCl_4$). Rates are obtained by analysis of the dielectric spectra (ω_{RBM}, $\omega_{\mathrm{M''}}$, ω_α, $\omega_{\text{sub-}\alpha}$) and rheology ($\omega_\eta$). Lines correspond to fits by the VFT equation.

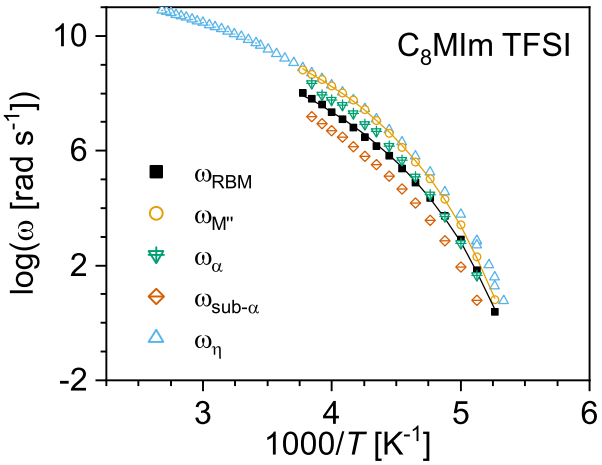

Figure 23: Temperature-dependent relaxation rates of the 1-octyl-3-methylimidazolium bis(trifluoromethylsulfonyl)imide (C_8MIm TFSI). Rates are obtained by analysis of the dielectric spectra (ω_{RBM}, $\omega_{\mathrm{M''}}$, ω_α, $\omega_{\text{sub-}\alpha}$) and rheology ($\omega_\eta$). Lines correspond to fits by the VFT equation.

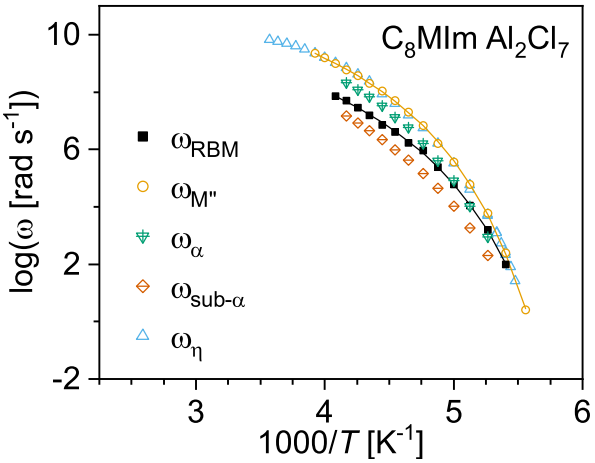

Figure 24: Temperature-dependent relaxation rates of the 1-methyl-3-octylimidazolium heptachlorodialuminate (C_8MIm Al_2Cl_7). Rates are obtained by analysis of the dielectric spectra (ω_{RBM}, $\omega_{\mathrm{M''}}$, ω_{α}, $\omega_{\text{sub-}\alpha}$) and rheology ($\omega_{\eta}$). Lines correspond to fits by the VFT equation.

References

References

(1) Kremer, F.; Schönhals, A. *Broadband Dielectric Spectroscopy*; Springer, Berlin, 2003; p 729.